

Morphological changes during the order-disorder transition in the two- and three-dimensional systems of scalar nonconserved order parameters

Marcin Fiałkowski¹ and Robert Hołyst^{1,2}

¹*Institute of Physical Chemistry, Polish Academy of Sciences, Kasprzaka 44/52, 01-224 Warsaw, Poland*

²*Department of Mathematics and Natural Sciences, College of Science, Cardinal Stefan Wyszyński University, Dewajtis 5, 01-815 Warsaw, Poland*

(Received 10 May 2002; published 21 October 2002)

The order-disorder transition is studied in a system of a scalar nonconserved order parameter. We use this well studied system to show that the application of the methods of topology and geometry reveals that our knowledge of the kinetic pathways by which the order-disorder transition proceeds is far from being complete. We show that in two-dimensional (2D) and 3D systems there are three dynamical regimes in the evolution of the system: early, intermediate, and late. In the intermediate regime two length scales govern the behavior of the system, whereas in the early and intermediate regime there is only one length scale. The size distribution of the domain area indicates the pathway by which the domains change their size. There are only two types of domains in a 2D system: circular and elongated with well defined characteristics (scaling of the area with the contour length) which in the late regime do not depend on time after rescaling by the average area and contour in the system. The elongated domains continuously change into circular domains reducing in this way the overall dissipation in the system. In order to reach a Lifshitz-Cahn-Allen (LCA) late stage regime the number of elongated domains must be strongly reduced. In the intermediate regime the number of elongated domains is large and simple LCA scaling does not hold. In a 3D symmetric system we always have a bicontinuous structure that evolves by cutting small connections. The late stage regime seems to be associated with the appearance of the preferred nonzero mean curvature. The early-intermediate regime crossover is associated with the saturation of the order parameter inside the domains, while the intermediate-late stage regime crossover is related to the global breaking of the \pm order parameter symmetry (marked by the appearance of the nonzero mean curvature but still zero average magnetization). The times for the occurrence of these crossovers do not depend on the size of the system.

DOI: 10.1103/PhysRevE.66.046121

PACS number(s): 64.60.Cn, 68.55.Jk, 75.40.Gb, 75.40.Mg

I. INTRODUCTION

Interfaces are ubiquitous in nature as they invariably form during typical phase transitions, such as paramagnetic-ferromagnetic, liquid-gas, liquid-solid, isotropic-nematic, uniform blend-separated blend, etc. In each case during the transition the domains of one phase appear and together with the domains an interface can be defined. Despite the fact that the kinetic pathways crucially depend on the curvature of the interfaces present in the system, not much attention has been paid in the domain of phase transitions to the morphology (topology and geometry) of these interfaces. This paper presents a thorough investigation of the system morphology in the simplest case of the phase transition, order-disorder phase transition in the system of the scalar nonconserved order parameter, and is a long version of our previous short paper [1]. Such system is a toy model for the paramagnetic-ferromagnetic phase transition.

As we have already stated, the simplest example of a system exhibiting the phase ordering kinetics [2–5] is a ferromagnet quenched from a temperature above its critical temperature T_c to a temperature below T_c . After lowering the temperature, such a system is brought into thermodynamically unstable, two-phase region. The two phases are characterized by positive and negative magnetizations, respectively. The system starts to evolve towards one of the two equilibrium states. Since both the coexisting \pm phases

are equally likely to appear, the system consists of domains of these two phases. During the phase ordering process the domains coarsen and the system orders over larger and larger length scales. The coarsening process is associated with the topological transformation of the interface. In order to describe quantitatively the latter one uses the Euler characteristic and/or genus, because they describe quantitatively the topology of the surface. The genus g of a closed surface is equal to the number of holes in it. The Euler characteristic is defined as $\chi = 2(1 - g)$. It is 2 for a sphere (since $g = 0$), 0 for a torus ($g = 1$), and -2 for two tori joined by a handle (passage) ($g = 2$). The Euler characteristic for a system of disjoint surfaces is equal to the sum of the Euler characteristic of individual surfaces. If we join two surfaces by a passage the Euler characteristic of a system will change by -2 , which is easy to see. Let us take two spheres for which we have $\chi = 4$. If we join them by a passage we will get a single closed surface with $\chi = 2$. Therefore a passage changed χ of the system by -2 . If a droplet appears in a system the Euler characteristic changes by $+2$. Therefore we have two typical topological elements: a droplet and a passage. Finally, it is possible to define the Euler characteristic for the flat interface in a periodic box. Such surface is equivalent topologically to a tori and therefore its Euler characteristic is zero. In our case of phase ordering the interface between the $+$ domains and the $-$ domains has a large and negative Euler characteristic at the beginning of the ordering

process, as the interface is highly interconnected and the initial structure is bicontinuous. At the end of the process the Euler characteristic is $+2$ or 0 , since either we have at the end a disappearing droplet of $+$ phase in the sea of $-$ phase or a flat interface between \pm phases.

The systems undergoing phase transitions (such as order-disorder transition) often exhibit scaling phenomena [2–5], i.e., a morphological pattern of the domains at earlier times looks statistically similar to a pattern at later times apart from the global change of scale implied by the growth of $L(t)$ —the domain size. Quantitatively it means, for example, that the correlation function of the order parameter (density, concentration, magnetization, etc.),

$$g(\mathbf{r}, t) = g(\mathbf{r}/L(t)), \quad (1.1)$$

where

$$L(t) \sim t^n, \quad (1.2)$$

the characteristic length scale in the system, scales algebraically with time t with the exponent n different for different universality classes [2]. The Fourier transform of the correlation function gives the scattering intensity that can be represented by the following scaling form:

$$I(k, t) = L^d(t) Y(kL(t)), \quad (1.3)$$

where k is the scattering wave vector and Y is the scaling function. Assuming the scaling hypothesis we can also derive all the scaling laws for different morphological measures, such as the Euler characteristic $\chi(t)$, surface area $S(t)$, the distribution $P_H(H, t)$ of the mean, and the Gaussian $P_K(K, t)$. It is interesting to note that these morphological measures allow a very detailed test of the scaling as we shall present in the paper. They also allow one to study the kinetic pathways by which various scaling regimes are achieved.

Despite the fact that the two-dimensional (2D) system of scalar nonconserved order parameter has been studied for almost 40 years [6], surprisingly, its morphology has only been determined *quantitatively* recently [7]. The domain structure can be in a first approximation viewed as a cellular structure. Cellular structures in 2D are known in many areas of science [8]. Whether we consider bee's honeycomb, soap foam (or froth) [9–11], defect condensation of charge density waves [12], territory of fire ants [13], administrative divisions [14,15], superclusters of galaxies (large scale structure of the universe) [16], 2D sections of polycrystalline materials, chemical patterns on surfaces or crack structure in ceramics [17], we find characteristic morphological patterns. Here we show that the domain pattern of the phase ordering systems in 2D obtained in our computer simulations defines a new 2D morphological class. Moreover, we will show how to obtain this morphology from the Jaynes maximum entropy principle [18] and show how to apply this principle to other 2D systems undergoing phase transitions.

Some progress in the study of morphology has been done in recent years both in the theoretical and experimental studies. The topological methods have been used for the classification of the extremely complex structures corresponding

to the local minima of the Landau-Ginzburg Hamiltonian [19–22] for the surfactant systems. It has been also shown that the phase transitions in the systems of surfactants (or in general in systems with internal surfaces) are accompanied by strong topological fluctuations that manifest themselves in a large peak of the standard deviation of the Euler characteristic at the transition and in the jump in the characteristic itself [23–26]. Such topological fluctuations have been also determined in the experiments for surfactant systems [27–29] since they strongly affect the rheological properties of such systems. Another application has been found in the study of the droplet-bicontinuous morphological transformation in the homopolymer blends [30,31] and the spinodal decomposition in mixtures [30,32,33]. The summary of other applications of the morphological measures can be found in the review articles [34–40]. The morphological studies in the experiments have been hampered by the lack of adequate methods for the reconstruction of three-dimensional images during the phase transitions. A great progress has been done recently. Jinnai *et al.* [41–43] from Hashimoto group developed a technique for the direct visualization of the interface in the 3D polymer system undergoing spinodal decomposition. From the 3D image obtained by the use of the laser scanning confocal microscopy (LSCM) the authors were able to obtain the curvature distribution of the interface and the scaling of the Gaussian and mean curvatures. The same authors combined the methods for the 3D reconstruction developed in LSCM experiments with spinodally decomposing blends and transmission electron microtomography to visualize the 3D structure of the gyroid phase in the triblock copolymer system and to measure its distribution of curvatures [44]. It is the purpose of this paper to show that topological and geometrical methods are indispensable tools in the study of phase transitions even in the simplest system such as a 2D and 3D phase ordering systems of the scalar nonconserved order parameter.

The paper is organized as follows. In the following section we will discuss the equations for the scaling of various morphological quantities. In Sec. III we will describe in detail the methods that allow computation of the interface area, Euler characteristic, and the Gaussian and mean curvatures. Next we will present the results for the order-disorder phase transitions in a 2D and a 3D system of the scalar nonconserved order parameter using the Landau-Ginzburg free energy and fully dissipative dynamics. The concluding remarks are contained in the summary.

II. ORDER-DISORDER TRANSITION: GROWTH EXPONENT AND DYNAMICAL SCALING

The dynamics of the system of the nonconserved scalar order parameter $\phi(\mathbf{r}, t)$ following a quench from the temperature $T = \infty$ to $T = 0$ is governed by the time dependent Ginzburg-Landau (TDGL) equation [2,6,45]:

$$\frac{\partial \phi(\mathbf{r}, t)}{\partial t} = - \frac{\delta F[\phi]}{\delta \phi}, \quad (2.1)$$

with the free-energy functional taken to have the form of the coarse-grained Ginzburg-Landau free energy,

$$F[\phi] = \int d\mathbf{r} \left[\frac{1}{2} |\nabla \phi(\mathbf{r})|^2 + f(\phi(\mathbf{r})) \right]. \quad (2.2)$$

The bulk potential $f(\phi)$ has the Landau-Ginzburg double-well structure

$$f(\phi) = \frac{1}{4} \phi^4 - \frac{1}{2} \phi^2, \quad (2.3)$$

with two degenerate minima at $\phi = \pm 1$. The TDGL equation with the potential given by Eq. (2.3) leads to the following kinetic equation governing the time evolution of the field $\phi(\mathbf{r}, t)$:

$$\frac{\partial}{\partial t} \phi(\mathbf{r}, t) = \Delta \phi(\mathbf{r}, t) + \phi(\mathbf{r}, t) - \phi^3(\mathbf{r}, t), \quad (2.4)$$

where Δ stands for the Laplacian.

The early stage of the phase ordering kinetics is governed by the saturation of the order parameter inside the domains. The phase interface then follows the bulk evolution and the exponent $n=0.5$ results simply from the linearized TDGL equation. If we drop the ϕ^3 term in Eq. (2.4), the solution $\phi_{\mathbf{k}}(t)$ in the Fourier space reads

$$\phi_{\mathbf{k}}(t) = \phi_{\mathbf{k}}(0) \exp[-(k^2 - 1)t], \quad (2.5)$$

where $k = |\mathbf{k}|$; the function $\phi_{\mathbf{k}}(0)$ is assumed to be a constant, and this corresponds to the initial conditions with the uncorrelated field $\phi(\mathbf{r}, 0)$. Since in the early stage the average domain size is very small, we have $k \gg 1$ and the argument of the exponent in Eq. (2.5) can be approximated by $-k^2 t$. The linearized equation (2.4) describes then a purely diffusive process and its real space solution is written as

$$\phi(\mathbf{r}, t) \sim \exp(-\mathbf{r}^2/4t) \equiv \exp\{-[\mathbf{r}/L(t)]^2\}. \quad (2.6)$$

In view of the above solution, it is clear why in the early stage of the evolution the characteristic length scale $L(t)$ grows as $t^{1/2}$.

Once the domains are saturated the system is supposed to enter the late stage scaling regime, where the whole evolution of the system is governed by one length scale $L(t)$, the size of the domains. It follows from Eq. (2.2) that, when inside the domain $\phi = \pm 1$, i.e., the domains are saturated, the coarsening of the domains is driven by the curvature of the domains [2,6]. The interface is defined by $\phi(\mathbf{r}, t) = 0$ and the local velocity of the interface is given by the local mean curvature of the interface, H :

$$v = -H. \quad (2.7)$$

It follows that all convex domains decrease their size. The typical time needed to close the domain of size $L(t)$ is $t \sim L(t)/v = L(t)/H_{char}$, where H_{char} is the characteristic curvature in the system. Now if $H_{char} \sim 1/L(t)$, we find $L(t) \sim t^{1/2}$ in the late stage regime. Please note that we need a characteristic mean curvature scaling in order to have the growth exponent 0.5.

The scaling relations (1.1), (1.2), and (1.3) have been recently supplemented by additional scaling relations for the morphological measures [1]. Assuming the scaling hypothesis, we can derive all the scaling laws for different morphological measures, such as the Euler characteristic $\chi(t)$, surface area $S(t)$, the distribution $P_H(H, t)$ of the mean, and the Gaussian $P_K(K, t)$ curvatures. The scaling hypothesis implies the following scaling laws for any phase separating/ordering symmetric system irrespective of the universality class:

$$S(t) \sim L(t)^{-1}, \quad (2.8)$$

$$\chi(t) \sim L(t)^{-d}, \quad (2.9)$$

$$P_H(H, t) = P_H^*(HL(t))/L(t), \quad (2.10)$$

$$P_K(K, t) = P_K^*(KL(t)^{(d-1)})/L(t)^{(d-1)}, \quad (2.11)$$

where d is the dimensionality of the system. The first law follows from the congruency of the domains [46]. We can, namely, treat the domains as spheres of diameter $L(t)$ touching each other. The total number of domains, n_d , is then $n_d = [L_0/L(t)]^3$, where L_0 denotes linear size of the system. Since the total area of the interface is proportional to the product $n_d L(t)^2$, the scaling relation (2.8) is obtained. The scaling law (2.9) results from the Gauss-Bonnet theorem, that relates the Euler characteristic to the Gaussian curvature and the surface area,

$$\chi = \gamma \int K(S) dS, \quad (2.12)$$

where $\int dS$ denotes the integral over the surface, and γ is twice the inverse of the volume of a $(d-1)$ -dimensional sphere of unit radius ($\gamma = 1/2\pi$ for $d=3$). Since

$$K(t) \sim L(t)^{-d+1} \quad (2.13)$$

and $S(t) \sim L(t)^{-1}$, we find scaling (2.9). The probability densities $P_H(H, t)$ and $P_K(K, t)$ are normalized to unity. The relation (2.10) is a simple consequence of the scaling of the mean curvature

$$H(t) \sim L(t)^{-1}. \quad (2.14)$$

The last relation results from the scaling (2.13) of the Gaussian curvature. Note that for $d=2$, the scalings (2.10) and (2.11) are equivalent. If true scaling exists in the system, all these scaling relations should be satisfied.

III. MORPHOLOGICAL MEASURES AND COMPUTATIONAL TOOLS

Since the 3D morphology is more complicated to describe, we will start by describing the methods for this case and at the end we will briefly mention the methods for the 2D morphologies.

The scalar order parameter giving the \pm magnetization, $\phi(\mathbf{r}, t)$ is represented on a cubic lattice. The functional $F[\phi(\mathbf{r})]$ [Eq. (2.2)] becomes a function $F(\{\phi_{i,j,k}\})$ of N^3

variables, where $D=(N-1)h$ is the linear dimension of the cubic lattice, h is the lattice spacing, and $\{\phi_{i,j,k}\}$ stands for the set of all variables of the function. Each variable $\phi_{i,j,k}$ represents the value of the field $\phi(\mathbf{r})$ at the point $\mathbf{r}=(i,j,k)h$, where $i,j,k=1,\dots,N$. In order to get rid of the boundary effects we impose the periodic boundary conditions $\phi_{1,j,k}=\phi_{N,j,k}$, $\phi_{2,j,k}=\phi_{N+1,j,k}$, $\phi_{3,j,k}=\phi_{N+2,j,k}$, $\phi_{0,j,k}=\phi_{N-1,j,k}$, $\phi_{-1,j,k}=\phi_{N-2,j,k}$, and similar for y and z directions. The points outside the unit cell, given by the periodic boundary conditions, enter the functional through the calculations of derivatives of points at the boundary and near the boundary of the lattice, i.e., when at least one of the indices i, j or k is equal to $1, 2, N-1$ or N . The periodic boundary conditions also simplify the computations of various morphological measures. In the periodic box the surface is, in fact, closed. For example, a plane is topologically equivalent to a torus. Therefore the standard definition of the genus as a number of holes in a closed surface can be used.

The surface separating \pm domains is given by the following equation

$$\phi(\mathbf{r}=(x,y,z))=0, \quad (3.1)$$

the position of the surface $\phi(\mathbf{r})=0$ is determined by interpolation between the neighboring points of different sign. It is highly unlikely, because of numerical accuracy, that a value of the field $\phi(\mathbf{r})=\phi_{i,j,k}$ at the point $\mathbf{r}=(i,j,k)h$ on the lattice is exactly zero. Therefore the points of the surface have to be localized by interpolation between the neighboring sites of the lattice. If $\phi(\mathbf{r}_1=(i,j,k)h)=\phi_{i,j,k}<0$ and $\phi(\mathbf{r}_2=(i+1,j,k)h)=\phi_{i+1,j,k}>0$, then the point \mathbf{r}_0 , for which $\phi(\mathbf{r}_0)=0$, must lie between the points $\mathbf{r}_1=(i,j,k)h$ and $\mathbf{r}_2=(i+1,j,k)h$. Moreover, the location of \mathbf{r}_0 depends on the values of the field at the points \mathbf{r}_1 and \mathbf{r}_2 in the following way:

$$\mathbf{r}_0=\left(i+\frac{|\phi_{i,j,k}|}{|\phi_{i,j,k}-\phi_{i+1,j,k}|},j,k\right)h. \quad (3.2)$$

All points of the surface $\phi(\mathbf{r})=0$ are found by the interpolation of the points located between the neighboring lattice sites. Due to the discretization, the unit cell is divided in $(N-1)^3$ small cubes of the size of the lattice spacing h . The surface $\phi(\mathbf{r})=0$ passing through a small cube cuts a polygon out of it. The edges of the polygons are formed by intersection of the surface and the faces of the small cube [21]. The edges can be approximated by straight lines. Unfortunately, the cube lattice decomposition scheme suffers from arbitrary choices, i.e., such representation of the surface leads to ambiguous situations. An alternative way to resolve the ambiguous surface approximations is to divide the original lattice not into cubes, but into more primitive subunits. Each cube can be divided into six five-vertex pyramids [40]. Here we use the simplest method based on the division of elementary cubes into tetrahedrons. When the tetrahedron decomposition is employed, the surface inside such simplex can be represented by only two cases (polygons): a triangle or a tetragon, as shown in Fig. 1. From the decomposition described above we can easily get the Euler characteristic χ . The practical

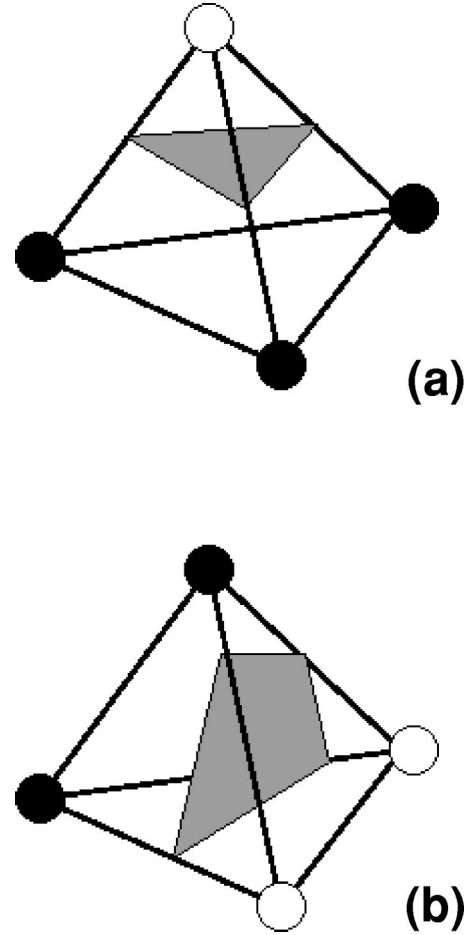


FIG. 1. Two cases of the polygonal surface representation in a single tetrahedron; a triangle (a) and a tetragon (b). The black and the white circles represent the points with the values of ϕ higher and lower than the threshold ϕ_0 .

way of computing χ is related to the coverage of the surface with polygons. Then, the calculation of the Euler characteristic is straightforward when it is based on the Euler formula:

$$\chi=\mathcal{N}_F+\mathcal{N}_V-\mathcal{N}_E, \quad (3.3)$$

where \mathcal{N}_F , \mathcal{N}_V , and \mathcal{N}_E are the number of faces, vertices, and edges respectively, of all polygons cut by the surface. The surface area is simply the area of all polygons covering the surface. Finally we can use the same polygons to compute the curvatures. Before we do it we present another method, which although imprecise, is frequently used [21]. From the differential geometry we have the following formulas for the curvatures.

$$H=-\frac{1}{2}\nabla\cdot\mathbf{n}=-\frac{1}{2}\nabla\cdot\left(\frac{\nabla\phi}{|\nabla\phi|}\right) \quad (3.4)$$

and

$$K=\frac{1}{2}[(\nabla\cdot\mathbf{n})^2-(\partial_i n_j)^2], \quad (3.5)$$

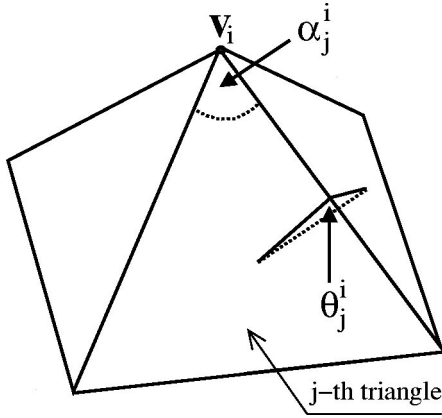


FIG. 2. A piece of polyhedron's surface composed of triangles meeting at the vertex v_i ; α_j^i is the angle between two edges of the j th triangle shearing the vertex v_i and θ_j^i is the angle between the faces of two adjacent triangles.

where \mathbf{n} is the vector normal to the surface at point \mathbf{r} , where we calculate the curvatures, and n_j is its j th component. Thus using the whole distribution of ϕ we can compute the distributions of curvatures. The errors produced by the use of the approximate formulas for the derivatives of ϕ are especially big if the spatial derivatives of the field ϕ have sharp peaks at the phase interface. This is a common situation in the late-stage kinetics of the phase ordering process, when the order parameter is saturated and the domains are separated by thin walls. There is, however, a simpler method that involves the previously defined polygons. It comes from integral geometry and does not suffer from the problems mentioned earlier.

Consider a polyhedron that is a discrete representation of the phase interface $\phi(\mathbf{r})=0$ obtained in the triangulation procedure. For each vertex of the polyhedron we can define the angle deficit by

$$T_i = 2\pi - \sum_{j=1}^m \alpha_j^i, \quad (3.6)$$

where m is the number of triangles that meet at i th vertex and α_j^i is the angle between the two edges of j th triangle at this vertex (see Fig. 2). The Gaussian curvature at i th vertex is given by

$$K_i \approx T_i / S_i, \quad (3.7)$$

where S_i is one-third of the area of the triangles. To prove this formula, let us first show that the integral of the Gaussian curvature over the surface region Σ_i (over triangles sharing the same vertex) is

$$\int_{\Sigma_i} K(S) dS = T_i. \quad (3.8)$$

The total angle deficit of the polyhedron, $T = \sum_{\{v_i\}} T_i$ is related to the number of its vertices \mathcal{N}_V , faces \mathcal{N}_F , and edges \mathcal{N}_E (Cartesian theorem) as

$$T = 2\pi(\mathcal{N}_V + \mathcal{N}_F - \mathcal{N}_E). \quad (3.9)$$

On the other hand, the total integral from the Gaussian curvature can be expressed by using the Gauss theorem:

$$2\pi(\mathcal{N}_V + \mathcal{N}_F - \mathcal{N}_E) = \int_{\Sigma} K(S) dS. \quad (3.10)$$

By using the fact that

$$\int_{\Sigma} K(S) dS = \sum_{\{v_i\}} \int_{\Sigma_i} K(S) dS \quad (3.11)$$

and comparing Eq. (3.9) to Eq. (3.10), Eq. (3.8) is deduced. Now, by assuming that the Gaussian curvature is constant within the region Σ_i , the formula (3.7) is obtained from Eq. (3.8).

The integral of the mean curvature H over the surface region Σ_i can be written as

$$\int_{\Sigma_i} H(S) dS = \tilde{H}_i, \quad (3.12)$$

where

$$\tilde{H}_i = \frac{1}{4} \sum_{j=1}^m l_j^i \theta_j^i; \quad (3.13)$$

l_j^i is the length of the edge of j th triangle and θ_j^i is the angle between two adjacent triangles j and $j+1$ (see Fig. 2). Assuming again the constancy of the mean curvature within the region Σ_i , its value can be evaluated as

$$H_i \approx \tilde{H}_i / S_i. \quad (3.14)$$

Note that in Eq. (3.13) the angles θ_j^i can have either sign, depending on the orientation of the surface of the polyhedron.

The curvature k of the interface in two dimensions is calculated in a similar way. Consider a polygon consisting of vertices v_i connected by edges l_i . Let us denote by l_i the length of the edge between $(i-1)$ th and i th vertex. The curvature k_i at the i th vertex can then be approximated as follows:

$$k_i \approx 2\theta_i / (l_i + l_{i+1}), \quad (3.15)$$

where θ_i denotes the angle between two edges that meet at the vertex v_i . Note also that the two-dimensional version of the Gauss-Bonnet theorem implies that the sum $\sum_i \theta_i$ taken over all vertices gives $\pm 2\pi$, where the sign depends on the orientation of the polygon boundary.

IV. COMPUTER SIMULATIONS AND RESULTS

Equation (2.4) has been solved on cubic 3D lattices of sizes 40^3 , 50^3 , and 100^3 and quadratic 2D lattices of sizes 512^2 , 1024^2 , and 2048^2 . All the quantities computed in the simulations have been averaged over 150 runs. A simple Euler integration scheme with time step $\Delta t = 0.05$ and mesh

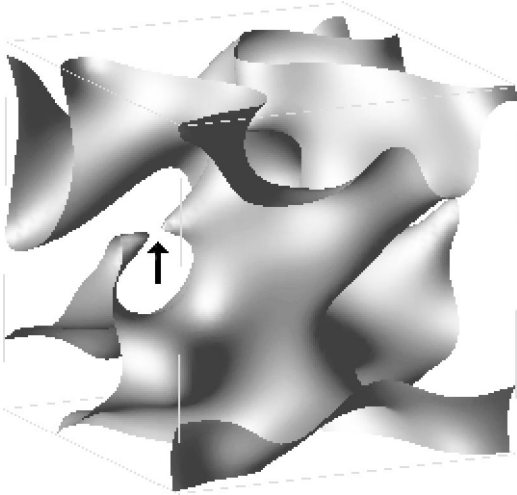


FIG. 3. Snapshot of the interface separating the $\phi < 0$ and $\phi > 0$ regions in the 3D ferromagnet undergoing the phase separating/ordering process. During the whole evolution the system has a bicontinuous morphology with a single interface and two percolating \pm domains. The arrow indicates remainings of the passage shortly after its breakage.

size $\Delta x = 1$ has been used. The initial conditions have been chosen from the uniform distribution of field ϕ with zero mean. In order to check the results against numerical artifacts we have varied the mesh size between $\Delta x = 0.5$ and 2 and also used different numerical approximations for the Laplacian with no apparent changes in the obtained results.

At every time step we determine the position of the interface separating the \pm domains. The interface given by the equation $\phi(\mathbf{r}) = 0$ is located (on the cubic lattice) by the linear interpolation of field ϕ between the lattice points. We find in 3D systems that after the initial transient time with many separated interfaces we get into the regime where there is a single surface in the system separating $\phi > 0$ domain from $\phi < 0$ domain. The \pm domains percolate and the system is bicontinuous in 3D (Fig. 3) and we have many closed domains in 2D (Fig. 4).

To derive $L(t)$ and the growth exponent n , we determine the equal time correlation function: $g(\mathbf{r}, t) = \langle \text{sgn}[\phi(\mathbf{r}, t)] \text{sgn}[\phi(0, t)] \rangle$ for which an approximate, analytical formula exists, given by Otha, Jasnov, and Kawasaki [47]:

$$g(\mathbf{r}, t) = \frac{2}{\pi} \arcsin\{\exp[-\mathbf{r}^2/L(t)^2]\}. \quad (4.1)$$

Fitting the simulation data to Eq. (4.1) we obtain the domain size $L(t)$.

A. 3D system: Domain size, curvatures, and the Euler characteristic

It was found in Refs. [1,48] that the system described by the TDGL equation exhibits two scaling regimes: (i) the early regime where the characteristic domain size $L(t)$ scales with $t^{0.5}$ and (ii) the intermediate regime where $L(t) \sim t^{0.4}$. The function $L(t)$ obtained from the relation (4.1) for the

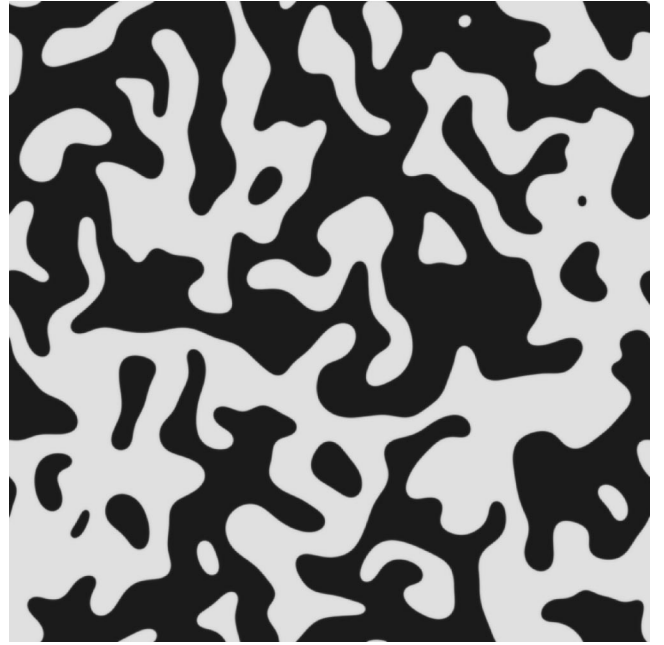


FIG. 4. Snapshot of the domain pattern in the 2D ferromagnet undergoing the phase separating/ordering process. The black and white colors represent, respectively, domains with positive and negative magnetizations.

system of size 100^3 is shown in Fig. 5. The transition between the early and the intermediate regimes was found to be marked by the saturation of the order parameter inside the domains. The crossover from the early to the intermediate stage occurs at $t_1 \approx 8.5$. The late-stage dynamics predicted by the Lifshitz-Cahn-Allen (LCA) theory with the growth exponent $n = 0.5$ was not observed by us in 3D due to finite-size effects, but it has been only recently observed for the system of 700^3 size by Brown and Rikvold [49]. The authors cited that the late stage in the 3D system is reached for $t \geq 150$. The growth of the domain size in the intermediate stage is not based on a single exponent. The effective exponent in this regime changes smoothly to 0.5 at the crossover time $t_2 \approx 150$ when the late stage begins. For the period $t_1 < t < 75$, the effective exponent derived from the simulation is $n = 0.40 \pm 0.02$.

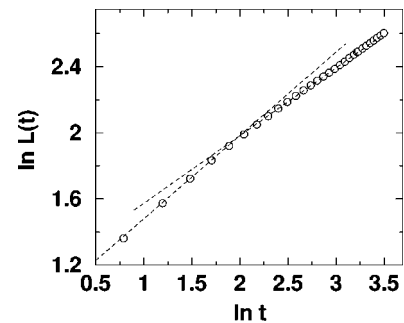


FIG. 5. Log-log plot of the time dependence of the domain size $L(t)$ for the 3D system. The least-squares fit yields the effective growth exponent 0.5 ± 0.01 in the early regime and 0.4 ± 0.02 in the intermediate regime. The crossover time $\ln t_1 \approx 2.1$ is marked by the saturation of the order parameter inside the domains [see Fig. 7(c)].

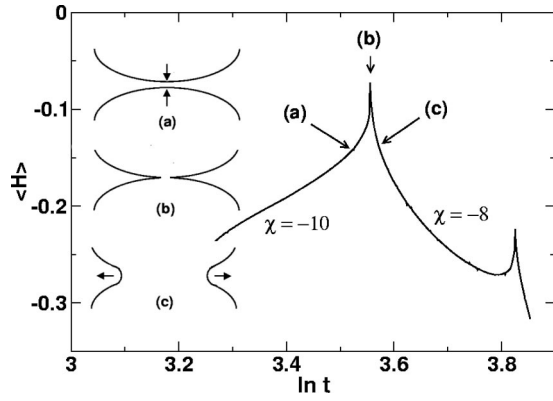


FIG. 6. Semilogarithmic plot of the time evolution of the average mean curvature $\langle H \rangle$ for a single run. The peaks correspond to the breakages of single passages. Three subsequent stages of the breakage of the passage are indicated: narrowing of the passage's neck (a), splitting of the passage into two separated pieces (b), and flattening out of the passage remainings towards the domain walls (c).

During the whole evolution the system has a *bicontinuous* morphology with a single interface and two percolating \pm domains in a 3D symmetric ordering system. At the beginning of the process the interface is highly interconnected by passages and has a large and negative Euler characteristic. As the phase separation proceeds, the number of passages decreases, which results in the increase of χ . Eventually, at the end of the process, the Euler characteristic is equal to 0 since in the final equilibrium state there is only one phase corresponding to negative or positive magnetization.

The curvature on the passage's neck is described by two principal radii R_n and R_s , where R_n is the radius of the neck and R_s denotes radius of the axial cross section of the passage's surface. The radii have opposite signs and the magnitude of R_n is much smaller than R_s . The local mean curvature on the neck $H = (1/R_n + 1/R_s)/2 \approx 1/2R_n$ tends to infinity as the neck narrows. Thus, the breaking of a single passage is accompanied by a rapid increase (or rapid decrease—depending on whether the neck's curvature $(1/2R_n)$ is positive or negative) of the total mean curvature $\langle H \rangle$. When the passage closes, its surface separates into two cone-shaped pieces. They are shown in Fig. 3 (indicated by the arrow). Since both pieces have pointed endings, according to Eq. (2.7), they flatten out quickly towards the domain walls. As a result, the excess curvature caused by the breakage of the passage is abruptly reduced. In Fig. 6 the average mean curvature $\langle H \rangle$ is plotted as the function of time. The peaks correspond to the breakages of single passages.

In Fig. 7 we show $\chi(t)$, $S(t)$, and $\langle |\phi(t)| \rangle$ as a function of time for three system sizes, 50^3 , 80^3 , and 100^3 . As we can see there is a clear change in the slope of $\ln \chi$ indicating the change of the scaling regime. In the early regime the exponent for χ is $-3/2$ (-1.53 ± 0.05) and in the intermediate regime it is -1 (-1.04 ± 0.05). For $S(t)$ we find the exponent $-1/2$ (-0.51 ± 0.01) in the first regime and $-2/5$ (-0.40 ± 0.01) in the second regime. The crossover time does not depend on the size of the system and from the plot of $\ln \langle |\phi| \rangle$ we find that it corresponds to the saturation of the

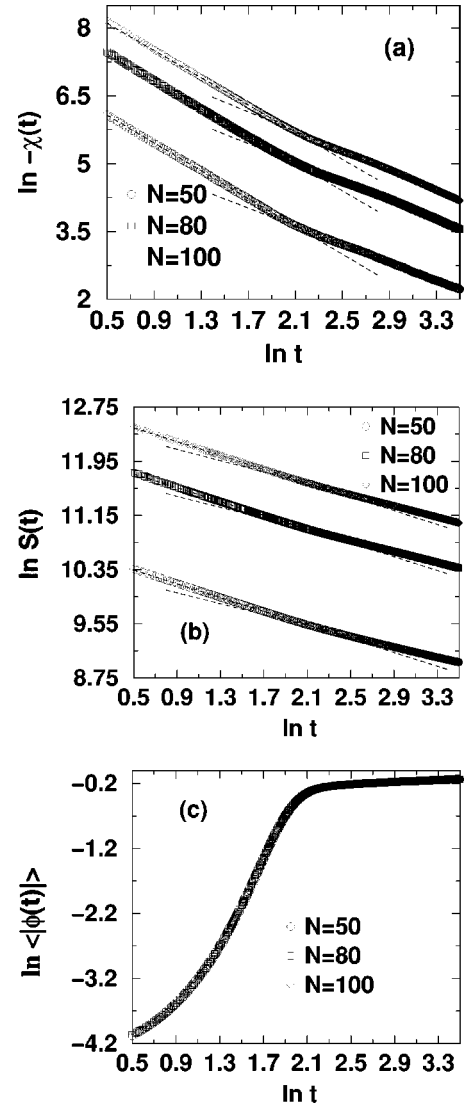


FIG. 7. The Euler characteristic χ (a), surface area S (b), and the order parameter inside the domains $\langle |\phi| \rangle$ (c) as a function of time t for the 3D system. The symbols correspond to system sizes $N = 50$ (\circ), 80 (\square), and 100 (\diamond). The dashed lines show the least-squares fits in the two scaling regimes. We find effective exponents of $-3/2$ and -1 for $\chi(t)$, and $-1/2$ and $-2/5$ for $S(t)$. The crossover time, $\ln t_1 \approx 2.1$, is marked by the saturation of the order parameter inside the domains as is evident from the plot (c).

order parameter (± 1) inside the domains. We have additionally analyzed the scaling of the principal curvatures obtained from the equations $H = (1/R_1 + 1/R_2)/2$ and $K = 1/(R_1 R_2)$ and found that $\langle 1/R_1 \rangle = 1/S \int dS/R_1 \sim -\langle 1/R_2 \rangle = -(1/S) \int dS/R_2 \sim 1/L(t)$ in the early regime and $\sim t^{-1/10}$ in the intermediate regime. We have also determined $\langle K \rangle / \sqrt{\langle 1/R_1^2 \rangle \langle 1/R_2^2 \rangle} \sim \text{const}$ in the early regime and $\sim t^{-1/2}$ in the intermediate regime. We also find that $\langle K \rangle \sim \langle 1/R_1 \rangle \langle 1/R_2 \rangle \sim 1/L(t)^2$ only in the early regime.

In Fig. 8 the histograms for the mean H and the Gaussian K curvatures are shown for the early regime. As we can see from this figure the scaling relations (2.10) and (2.11) are satisfied with $n = 0.50 \pm 0.01$. Scaling of the distributions of H and K in the intermediate regime are shown in Fig. 9. As

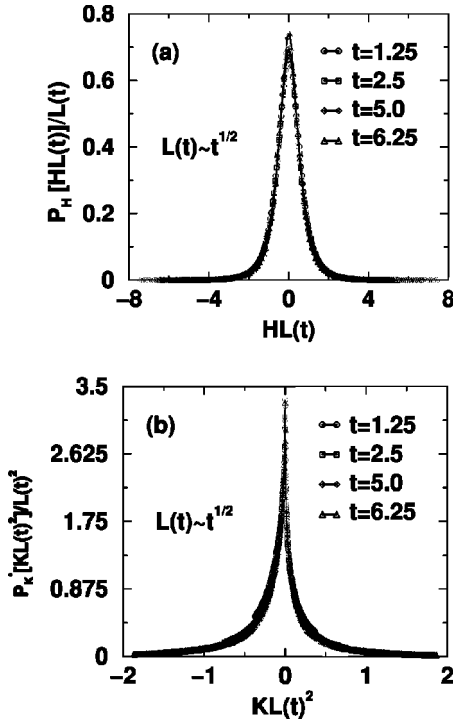


FIG. 8. Scaling of the mean H (a) and Gaussian K (b) curvatures (given in dimensionless units) in the early regime. The distributions obey the scaling relations (2.10) and (2.11) with the growth exponent $n=0.5$. The system size is 50^3 .

seen, for different times the data collapse onto single master curves. However, in contrast to the early regime, there is no single common length scale for the mean and Gaussian curvatures. The scaling relations (2.10) and (2.11) are satisfied with $n_H=2/5$ and $n_K=3/10$, respectively. Therefore, the curvatures H and K scale independently with two different length scales $L_H(t)$ and $L_K(t)$ that vary with time t as

$$L_H(t) \sim t^{2/5}, \quad (4.2)$$

$$L_K(t) \sim t^{3/10}. \quad (4.3)$$

In terms of the two quantities $L_H(t)$ and $L_K(t)$ the scaling relations (2.8)–(2.11) can be rewritten in the following form:

$$S(t) \sim L_H(t)^{-1}, \quad (4.4)$$

$$\chi(t) \sim L_K(t)^{-2} L_H(t)^{-1}, \quad (4.5)$$

$$P_H(H, t) = P_H^*(HL_H(t))/L_H(t), \quad (4.6)$$

$$P_K(K, t) = P_K^*(KL_K(t)^2)/L_K(t)^2. \quad (4.7)$$

Note that the second relation, Eq. (4.5), expresses the Gauss-Bonnet theorem (2.12), with the average Gaussian curvature $K(t) \sim L_K(t)^{-2}$.

In view of the four relations (4.4)–(4.7), we see that the length scale $L_H(t)$ can be interpreted as the *geometrical* measure of the phase interface. It determines quantities such as the characteristic domain size, the area of the interface, and the mean curvature. The second length scale $L_K(t)$ is

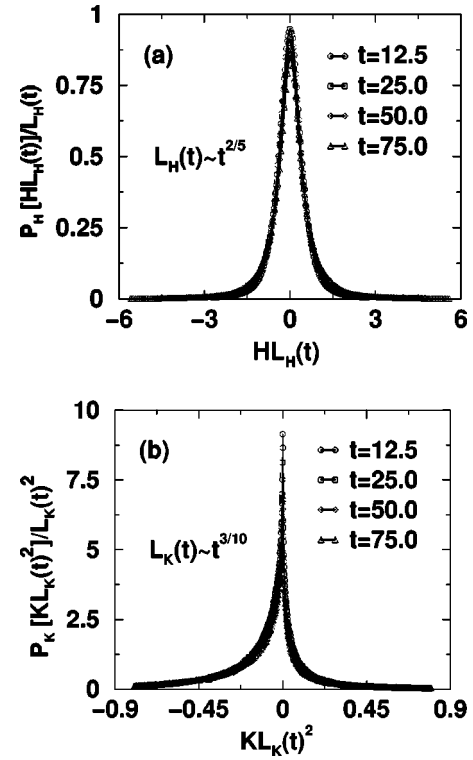


FIG. 9. Scaling of the mean H (a) and Gaussian K (b) curvatures (given in dimensionless units) in the intermediate regime. The scaling relations (2.10) and (2.11) are satisfied with the exponents $n_H=0.4$ and $n_K=0.3$, respectively. The system size is 50^3 .

related to the *topology* of the system and characterizes its Euler characteristic and the Gaussian curvature.

The existence of the two length scales in the intermediate regime has a simple physical interpretation and can be explained in terms of the LCA theory, that links the velocity of the interface with its local curvature. Below, we demonstrate that it is related to the domain-neck decoupling processes [1] taking place in the intermediate stage of the evolution. Let us denote by $n_d(t)$ the average number of domains in the system, which are assumed to be spheres of the diameter $L_H(t)$. The Euler characteristic is then proportional to the product

$$\chi(t) \sim n_d(t)p(t), \quad (4.8)$$

where $p(t)$ is the number of necks or passages piercing the surface of the sphere (connectivity). On the other hand, according to the Gauss-Bonnet theorem, the Euler characteristic can be written as $\chi(t) \sim K(t)S(t)$. Since the total area $S(t)$ of the interface is proportional to the product of the surface of the sphere of radius $L_H(t)$ and the number $n_d(t)$ of the domains, we get

$$\chi(t) \sim L_K(t)^{-2} n_d(t) L_H(t)^2. \quad (4.9)$$

By comparing Eqs. (4.8) and (4.9) we obtain

$$p(t) \sim \left(\frac{L_H(t)}{L_K(t)} \right)^2. \quad (4.10)$$

In the early regime we have $L_H(t) = L_K(t) = L(t) \sim t^{1/2}$ and, therefore, $p(t) \sim 1$ is independent of time. This means that for each sphere of size $L(t)$ we have the same number of passages. In the intermediate regime we have $L_H(t) \sim t^{2/5}$ and $L_K(t) \sim t^{3/10}$, which gives $p(t) \sim t^{1/5}$ indicating the decoupling between the domains and the connections joining them.

Since in the intermediate regime the average mean curvature is equal to zero and its distribution is peaked at $H=0$ [Fig. 9(a)], we deduce that the phase interface possesses large patches of the minimal-like (saddle like) shape [20,21] with zero mean curvature. Furthermore, the appearance of the domain-neck decoupling process indicates that these areas are localized mainly at the necks connecting the domains. This means that in the intermediate regime the necks are in “partially frozen” state and slow down the kinetics of the system. They evolve slower (with the exponent $n_K=0.3$) compared to the domains following the evolution with the growth exponent $n_H=0.4$. Of course, the LCA argument does not work in the intermediate regime. However, during the evolution, the morphology of the system changes and transforms successively from the “minimal-like” structure [with the mean curvature $H(t)$ equal to zero] to the “constant-mean-curvature-like,” where the average mean curvature is proportional to the inverse of the characteristic size of the domains, i.e., $H(t) \sim 1/L(t)$. Once the morphological transformation is completed the LCA argument works and the late scaling with the growth exponent $n=0.5$ is reached. To sum up, in the intermediate regime the evolution of the morphology of the phase interface splits off and the “geometry” and the “topology” start to evolve independently with two different growth exponents $n_H=0.4$ and $n_K=0.3$, respectively. This process manifests as the breaking down of the scaling laws, Eqs. (2.8)–(2.11). The existence of the two length scales in the intermediate regime is a consequence of the fact that the late-stage morphology and the early-stage morphology differ significantly and by no means can be transformed one into another by scaling operations based on a single length scale.

In order to monitor behavior of the connectivity index $p(t)$ during the phase ordering process we use the following relation:

$$p(t) = -\frac{\chi(t)}{S(t)^3}, \quad (4.11)$$

which follows immediately from Eqs. (4.4), (4.5), and (4.10). In Fig. 10 the time evolution of the quantity $p(t)$, calculated from Eq. (4.11), is plotted. As seen, in the early stage $p(t)$ hardly changes, which confirms the prediction that $p(t)$ remains constant before the order parameter has saturated. Next, in the intermediate stage, its value starts to grow. The growth exponent is roughly 0.2. This value of the growth exponent is in agreement with the prediction $n=2(n_H - n_K)=0.2$ following from Eq. (4.10). We see that $p(t)$ starts to saturate for $t \geq 100$ signaling the end of the topological transformation discussed above. We also expect that the value $p(t) \approx 0.26$ attained at the end of the intermediate stage

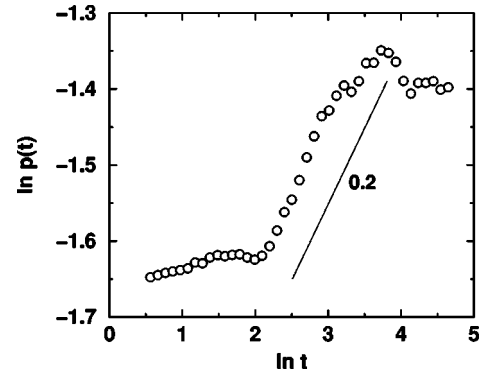


FIG. 10. Time evolution of the connectivity index $p(t) = -\chi(t)/S(t)^3$ plotted on a log-log scale.

does not change during the late stage (not observed in our simulations due to the finite-size effects).

It is worth noting here that the parameter $p(t)$ calculated from Eq. (4.11) is related to some existing measures used to characterize features of minimal surfaces. Namely, the quantity $\mathcal{G} = 2S_0^3/\pi\chi_0$, referred to as the dimensionless group, was applied [50] to describe various types of triply periodic minimal surfaces [20,21] with respect to their topology. S_0 and χ_0 denote here, respectively, the surface area and the Euler characteristic calculated for unit cell. Another quantity used to characterize minimal surfaces is the so-called homogeneity index \mathcal{H} [51] defined as $\mathcal{H} = S^{3/2}/|2\pi\chi|^{1/2}V$, with V being the volume of the unit cell. The dimensionless group and the homogeneity index are linked with the parameter $p(t)$ by the relation $\mathcal{H} \sim \mathcal{G}^{1/2} \sim p^{-1/2}$.

B. 2D system: Scaling regimes

In Fig. 11 the average domain size calculated from Eq. (4.1) for the 2D system of size 2048^2 is plotted. It follows from Fig. 11 that the evolution of the system can be divided

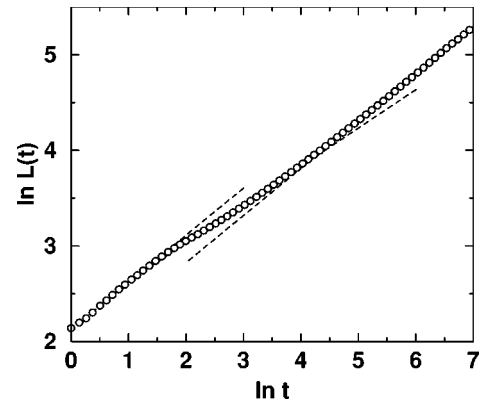


FIG. 11. Log-log plot of the time dependence of the domain size $L(t)$ for the 2D system of size 2048^2 . The least-squares fit to the data points in the early regime gives the growth exponent $n=0.49 \pm 0.01$. In the intermediate regime, for the period of time $2.1 < \ln t < 4$, $n=0.40 \pm 0.02$. In the late stage, for $t \geq 150$, the growth exponent is $n=0.49 \pm 0.01$. The transition between early and intermediate stages is marked by the saturation of the order parameter inside the domains [see Fig. 12(c)].

into three scaling regimes: early, intermediate, and late. The least-squares fit yields the growth exponent $n = 0.49 \pm 0.01$ in the early stage and $n = 0.40 \pm 0.02$ in the intermediate stage for the period of time $2.1 < \ln t < 4$. The transition from the early to the intermediate stage is marked by the saturation of the order parameter inside the domains [see Fig. 7(c)]. The late stage is reached when the growth exponent n attains the value of 0.5 (0.49 ± 0.01) predicted by the LCA theory. The crossover time t_2 from intermediate to the late stage is roughly $t_2 \approx 150$. Note that the same value of the crossover time t_2 has also been found [49] for the 3D system.

In Fig. 12 the total number of objects (closed contours) in the system, $N(t)$, the total length of the phase interface (border line) $C(t)$, and the saturation of the order parameter inside the domains, $\langle |\phi| \rangle$, are shown. The number of objects, N , plays here a role of the 2D version of Euler characteristic. The scaling relations for $N(t)$ and $C(t)$ have the following form in 2D:

$$C(t) \sim L(t)^{-1}, \quad (4.12)$$

$$N(t) \sim L(t)^{-2}. \quad (4.13)$$

We have found that in the early stage the number of contours, $N(t)$, grows with the effective exponent $n_N = -1.02 \pm 0.01$, and the length of the interface with the exponent $n_C = -0.51 \pm 0.01$. The scaling relations (4.12) and (4.13) with the growth exponent $n = 0.5$ are therefore satisfied. In the late regime, for $\ln t > 6$, we found that $N(t)$ scales with the growth exponent -0.98 ± 0.01 and $C(t)$ scales with the exponent -0.49 ± 0.01 . Thus, in the late stage the scaling relations are satisfied with the growth exponent $n = 0.5$. In the intermediate stage the growth exponent changes gradually from the value of 0.4 at the beginning to 0.5 as the evolution enters the late regime. However, for the period of time $t_1 < t < 55$ the slope of the curves plotted in Figs. 12(a) and 12(b) do not change much and one may determine effective exponents for $N(t)$ and $C(t)$. Least-squares linear fits to the data points yield $n_N = -0.84 \pm 0.02$ and $n_C = -0.41 \pm 0.01$. This means that the scaling holds with a good approximation in the intermediate regime with the effective growth exponent $n = 0.4$.

The growth exponent 0.4 obtained for the intermediate regime indicates slowing down of the evolution after the early stage. As in the case of the 3D system analyzed in the preceding section, this fact can be explained by the morphology of the domain pattern formed after the order parameter has saturated inside the domains. In the early stage the evolution of the system is diffusive and the exponent 0.5 follows from Eq. (2.6). Once the magnetization saturates and the domain walls get thin, further evolution of the system is driven by the curvature of the interface. As we shall demonstrate in the following section, at the beginning of the intermediate stage, the domains mostly have elongated shapes. The phase interface is composed of great amount of immobile, almost straight lines (of zero curvature), that slow down the curvature-driven kinetics.

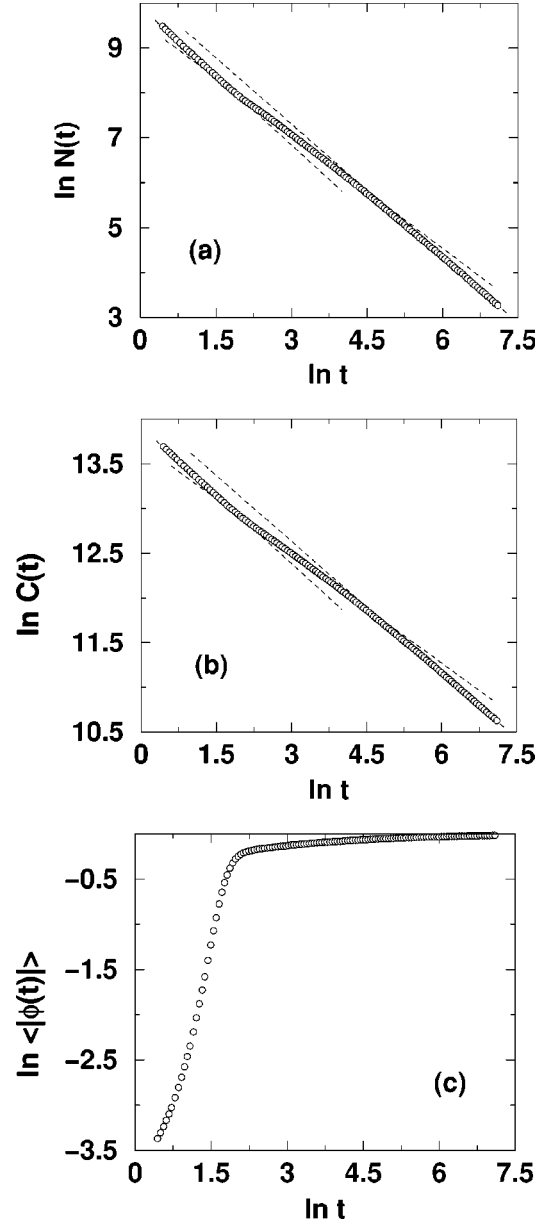


FIG. 12. The total number of objects N (a), the total length of the borderline C (b), and the saturation of the order parameter inside the domains, $\langle |\phi| \rangle$ (c), as functions of time t for the 2D system of size 2048^2 . The dashed lines represent the least-squares fits in the three scaling regimes. The crossover time, $\ln t_1 \approx 2.1$, between early and intermediate stages is marked by the saturation of the order parameter inside the domains. In the early stage the effective growth exponents are $n_N = -1.02 \pm 0.01$ and $n_C = -0.51 \pm 0.01$; in the intermediate stage (for $\ln t_1 < \ln t < 4$) $n_N = -0.84 \pm 0.02$ and $n_C = -0.41 \pm 0.01$; in the late stage, for $\ln t > 6$, $n_N = -0.98 \pm 0.01$ and $n_C = -0.49 \pm 0.01$.

C. Domain size distribution

In order to study the shapes of the domains we have triangulated them and computed for each domain its area s and length of the interface l at each time step of the evolution. Next we computed the average values of their area and interface length, $s_{av}(t)$ and $l_{av}(t)$, as a function of time. We have found that the shape of the domains exhibit the following scaling relation:

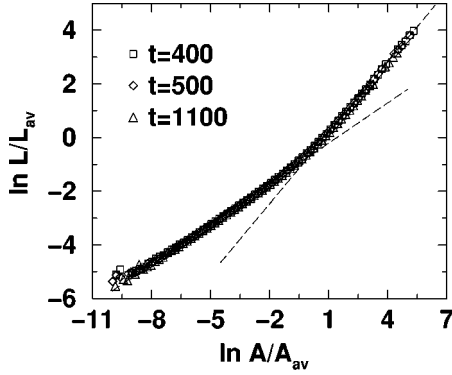


FIG. 13. The scaling relation between the interface length L and the domain area A during the process of phase ordering in 2D system. On this plot we put the results obtained for about 330 000 domains collected for three different times ($t=400, t=500, t=1100$). The master curve consists of two straight lines [Eqs. (4.14) and (4.15)] indicating two types of domains in the system.

$$l/l_{av}(t) \sim [s/s_{av}(t)]^\nu, \quad (4.14)$$

where the exponent ν depends on whether the domain area s is above or below the average $s_{av}(t)$:

$$\nu = \begin{cases} 0.50 \pm 0.01 & \text{if } s < s_{av}(t) \\ 0.88 \pm 0.01 & \text{if } s > s_{av}(t). \end{cases} \quad (4.15)$$

This scaling relation is shown in Fig. 13, where we have taken all the domain areas and interface lengths for three different times ($t=400, 500, 1100$) and more than 330 000 domains. It is remarkable that all the domains for all times fall onto a single master curve showing fairly high degree of regularity in the morphology of the system. In principle, for a highly irregular (chaotic) morphology we would see, instead of a single curve, many points scattered all over the diagram. This equation also shows that the system undergoing the phase ordering kinetics exhibits scaling at the level of the shapes of the domains. It means that the shapes of the domains at earlier times look statistically similar to the shapes at later times, apart from the global change of the average area and interface length.

It follows from Fig. 13 and Eq. (4.15) that in the late-stage regime we find in the system two types of domains: large and elongated ones with contour length proportional (roughly) to their area ($l^{1/0.88} \sim s$) and circular domains for which $l^2 \sim s$. The evolution follows a path along which the elongated domains change continuously into circular domains. In this way dissipation is reduced. In order to see it, let us consider the local energy change per unit time and unit length of the domain interface. This quantity is proportional [2] to v^2 , where the local velocity of the interface, $v = -H$. Integrating v^2 over the interface length of a domain gives the dissipation per domain. For a circular domain this dissipation is proportional to $1/l$ (since $H \sim 1/L \sim 1/l$), while for the elongated domain it is $1/l^{0.14}$. Therefore the change of shape of the domains during this evolution follows the kinetic pathway along which the dissipation is continuously reduced.

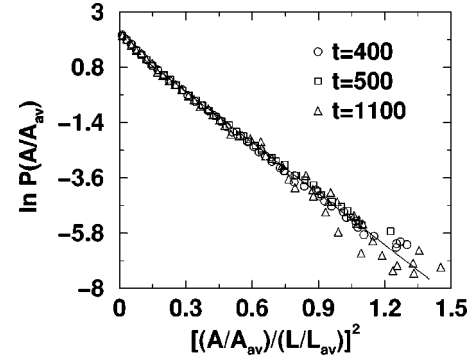


FIG. 14. The distribution function for the domain area in the late-stage regime. It is shown in the scaled form $p(A, t) \sim \exp[-\alpha(x/y)^\mu]$ with $\mu=2$, $x=A/A_{av}$, and $y=L/L_{av}$ for three different times (see Fig. 13). This fit strongly support the MEP conjecture with the entropy of $p(A, t)$ [Eq. (4.16)].

We have determined the distribution of sizes of the domains, $p(s, t)$. Following the conjecture made by Jaynes [18] we assumed that the distribution can be obtained from the maximum entropy principle with some additional constraints. We have found that the entropy [18]

$$\mathcal{S}(t) = - \int ds p(s, t) \ln p(s, t) \quad (4.16)$$

is maximized at each instant of time t subject to the condition

$$\int ds p(s, t) (s/l)^\mu = (\text{fixed}), \quad (4.17)$$

where $\mu=2$ and the dependence of l on s , which reflects the system dynamics, is given by Eqs. (4.14) and (4.15). The exponent μ can be deduced from the LCA theory. Because $s/l \sim L(t)$ (domain size) we conclude that the constraint sets the characteristic time $\tau \sim (L(t))^\mu \sim (s/l)^\mu$ proportional to the time needed to close the domain of size $L(t)$. From the LCA theory we have $\tau \sim L^2$ and consequently $\mu=2$. Similarly, for other systems undergoing phase transitions the exponent μ should follow from the growth of the average domain sizes. In this sense our analysis is robust and not restricted to the specific system under study.

From the maximization of the entropy $\mathcal{S}(t)$ [Eq. (4.16)] subject to the constraint (4.17), we find

$$p(s, t) = C(t) \exp[-\lambda(t)(s/l)^\mu]. \quad (4.18)$$

Using the scaling principle we find the distribution in the rescaled form:

$$p(x) = C^* \exp[-\lambda^*(x/y)^\mu], \quad (4.19)$$

where $x=s/s_{av}(t)$, $y=l/l_{av}(t)$, C^* and λ^* are constants independent of time, and $\mu=2$. Equation (4.19) is satisfied in the late-stage regime as shown in Fig. 14, where the distribution $p(x)$ obtained from the simulations is plotted. This gives a strong support to the application of maximum entropy principle to the kinetics of phase transition. Other distributions such as $p_1(l, t)$ can be obtained from $p(s, t)$ by the

change of variables, i.e., $p_1(l,t) = p(s(l),t) ds(l)/dl$. We note that the choice of the distribution in Eq. (4.16) is not trivial. For example, a possible choice of $p_1(l,t)$ would lead to the disagreement with our computer simulations. The analysis presented here for the kinetics of phase transitions leads additionally to the definition of the 2D morphology class that can be characterized by two exponents (μ and ν). Equations (4.16) and (4.17) form the basis of the general principle which governs the form of the distribution function while Eqs. (4.14) and (4.15) are characteristic for a given system.

V. SUMMARY

We have investigated the phase separating/ordering process in the 2D and 3D systems with nonconserved scalar order parameter. In our studies we have applied tools based on the topology and geometry of the phase interface. We have found that the evolution of the 2D and 3D systems can be divided into three regimes: early, intermediate, and late. In the early stage the evolution is diffusive and the domain growth is characterized by the exponent $n \approx 0.5$. The transition from the early to the intermediate stage is marked by the saturation of the order parameter inside the domains. The crossover time $t_1 \approx 8.6$ is similar for the 2D and 3D systems. In the intermediate stage the kinetics is driven by the curvature of the interface. It is slowed down, which manifests in the change of the effective growth exponent n from 0.5 in the early stage to, approximately, 0.4 at the beginning of the intermediate stage. This effect is due to the morphology of the domain structure formed at the end of the early stage. In the 3D system the phase interface possesses large patches of flat surfaces of minimal-like shape with zero local mean curvature. In the 2D system the domains have mostly elongated shapes with the borderline composed of a large number of almost straight lines. These immobile zero-curvature pieces of the interface are responsible for the slowing down of the phase separating/ordering kinetics taking place in 2D and 3D in the intermediate stage.

The observed scaling properties of the 3D system in the intermediate stage can be described in terms of two length scales $L_H(t)$ and $L_K(t)$. They characterize, respectively, scaling of the distributions of the mean H and Gaussian K curvatures. $L_H(t)$ varies with the time as $t^{0.4}$ and is related to the *geometrical* properties of the system such as the average size of the domains, the surface area, and characteristic radius of the curvature. The second length scale $L_K(t) \sim t^{0.3}$ is associated with the *topological* features of the system's interface and determines its Euler characteristic and the Gaussian curvature. The appearance of the two length scales is related to the domain-neck decoupling process and accompanies the morphological transformation from the minimal-like structure formed at the early stage to the constant-mean-curvature-like structure, which is characteristic of the late-stage dynamics. Although both the early- and the late-stage morphologies are bicontinuous, they differ significantly and the system cannot be brought from the early stage to the late stage by simple scaling. The topological changes can be monitored by the connectivity index $p(t)$ that remains con-

stant in the early and late regimes, and grows with the exponent 0.2 in the intermediate stage.

In the 2D system the transition from the intermediate to the late stage is also associated with the transformation of the domain morphology. Namely, at the beginning of the intermediate stage the elongated domains outnumber the circular ones. In the process the elongated domains continuously change into circular domains reducing in this way the overall dissipation in the system. In contrary to the 3D system, we do not have two length scales in 2D. This is understood since the Gaussian K and the mean H curvatures reduce to one curvature k in two dimensions and the scaling relations (2.10) and (2.11) become equivalent. However, in the case of elongated domains forming a system of meandering fingers (dendrits), two characteristic lengths are present, i.e., the characteristic width and length of the fingers. Thus, the transformation of the typical domain shape from elongated to circular one (based on one characteristic length scale—the size of the domain) is linked with elimination of one of the two length scales appearing in the intermediate stage.

The intermediate-late stage regime crossover is related to the global breaking of the \pm order parameter symmetry, which is marked by the appearance of the nonzero mean curvature but still zero average magnetization. Both the 2D and 3D systems reach the late-scaling regime at $t_2 \approx 150$.

The topology and the geometry of the interfaces in phase separating/ordering systems are accessible in the laser scanning confocal microscopy (LSCM) experiments (Refs. [41–44]). It shows that developing theoretical tools in this direction is relevant for experiments.

The methods presented in the paper are complementary to the standard tools, such as determination of the correlation function. In principle, one can even determine from the short distance behavior of the correlation function the average area per unit volume and the averaged curvatures. Such procedure has been already applied in light scattering experiments (standard technique) (Ref. [52]). We hope that in the future one can combine both approaches and find more common points, i.e., to see where the information about topology and geometry of interfaces is hidden in the correlation functions.

The methods presented in the paper are generic, i.e., are applicable to any system undergoing kinetics of phase transition. In fact, we have decided to put on our web page [53] the source code (free of charge) to be used for the determination of 3D and 2D morphology in systems with internal surfaces.

The use of the methods based on the geometry and topology of the interface has revealed that our knowledge of the kinetic pathways by which the order-disorder transition proceeds is far from being complete, even in the case of well studied system of a scalar nonconserved order parameter. We believe that the application of the morphological methods will be also fruitful in the study of phase transitions in other systems where the interface separating two phases exists.

ACKNOWLEDGMENTS

This work was supported by the KBN through Grant No. 5P03B09421.

- [1] M. Fiałkowski, A. Aksimentiev, and R. Hołyst, *Phys. Rev. Lett.* **86**, 240 (2001).
- [2] A.J. Bray, *Adv. Phys.* **43**, 357 (1994).
- [3] J.S. Langer, in *Solids far from Equilibrium*, edited by C. Godreche (Cambridge University Press, Cambridge, England, 1992), p. 297.
- [4] K. Binder, *Rep. Prog. Phys.* **50**, 783 (1987).
- [5] J.D. Gunton, M. San Miguel, and P. Sahni, in *Phase Transitions and Critical Phenomena* edited by C. Domb and J.L. Lebowitz (Academic Press, New York, 1983) Vol. 8, p. 267.
- [6] S.M. Allen and J.W. Cahn, *Acta Metall.* **27**, 1085 (1979); I.M. Lifshitz, *Zh. Eksp. Teor. Fiz.* **42**, 1354 (1962).
- [7] M. Fiałkowski and R. Hołyst, *Phys. Rev. E* **65**, 057105 (2002).
- [8] D. Weaire and N. Rivier, *Contemp. Phys.* **25**, 59 (1984).
- [9] J. Stavans and J.A. Glazier, *Phys. Rev. Lett.* **62**, 1318 (1989).
- [10] A. Hamsy, R. Paredes, O. Sonnevile-Aubrun, B. Cabane, and R. Botet, *Phys. Rev. Lett.* **82**, 3368 (1999).
- [11] A.A. Kader and J.C. Earnshaw, *Phys. Rev. Lett.* **82**, 2610 (1999).
- [12] H.H. Weitering, J.M. Carpinelli, A.P. Melechko, J.D. Zhang, M. Bartkowiak, and E.W. Plummer, *Science* **285**, 2107 (1999).
- [13] E.S. Adams, *Ecology* **79**, 1125 (1998).
- [14] G.L. Caër and R. Delannay, *J. Phys. I* **3**, 1777 (1993).
- [15] L. Glass and W.R. Tobler, *Nature (London)* **233**, 67 (1971).
- [16] P. Coles, *Nature (London)* **346**, 446 (1990).
- [17] W. Korneta, S.K. Mendiratta, and J. Menteiro, *Phys. Rev. E* **57**, 3142 (1998).
- [18] E.T. Jaynes, *Phys. Rev.* **106**, 620 (1957); **108**, 171 (1957).
- [19] W. Gózdź and R. Hołyst, *Macromol. Theory Simul.* **5**, 321 (1996).
- [20] W. Gózdź and R. Hołyst, *Phys. Rev. Lett.* **76**, 2726 (1996).
- [21] W. Gózdź and R. Hołyst, *Phys. Rev. E* **54**, 5012 (1996).
- [22] U.S. Schwarz and G. Gompper, *Phys. Rev. E* **59**, 5528 (1999).
- [23] R. Hołyst and W. Gózdź, *J. Chem. Phys.* **106**, 4773 (1997).
- [24] R. Hołyst and P. Oswald, *J. Chem. Phys.* **109**, 11 051 (1998).
- [25] R. Hołyst and P. Oswald, *Phys. Rev. Lett.* **79**, 1499 (1997).
- [26] R. Hołyst, *Curr. Opin. Colloid Interface Sci.* **3**, 422 (1998).
- [27] D. Constantin and P. Oswald, *Phys. Rev. Lett.* **85**, 4297 (2000).
- [28] D. Constantin, P. Oswald, M. Iperor-Clerck, M. Davidson, P. Sotta, and J. Phys. Chem. B **105**, 668 (2001).
- [29] D. Constantin, J.-F. Palierne, E. Freyssingeas, and P. Oswald, *Europhys. Lett.* **58**, 236 (2002).
- [30] A. Aksimentiev, K. Moorthi, and R. Hołyst, *J. Chem. Phys.* **112**, 6049 (2000).
- [31] A. Aksimentiev, R. Hołyst, and K. Moorthi, *Macromol. Theory Simul.* **9**, 661 (2000).
- [32] K. Mecke and V. Sofonea, *Phys. Rev. E* **56**, R3761 (1997).
- [33] V. Sofonea and K.R. Mecke, *Eur. Phys. J. B* **8**, 99 (1999).
- [34] K.R. Mecke, *Acta Phys. Pol. B* **28**, 1747 (1997).
- [35] K.R. Mecke, *Int. J. Mod. Phys. B* **12**, 861 (1998).
- [36] K. Michielsen and H. De Raedt, *Phys. Rep.* **347**, 462 (2001).
- [37] J.S. Kole, K. Michielsen, and H. De Raedt, *Phys. Rev. E* **63**, 016201 (2001).
- [38] K. Michielsen and H. De Raedt, *Comput. Phys. Commun.* **132**, 94 (2000).
- [39] K. Michielsen and H. De Raedt, *Phys. Rev. B* **59**, 4565 (1999).
- [40] A. Aksimentiev, M. Fiałkowski, and R. Hołyst, *Adv. Chem. Phys.* **121**, 141 (2002).
- [41] H. Jinnai, Y. Nishikawa, T. Koga, and T. Hashimoto, *Macromolecules* **28**, 4782 (1995).
- [42] H. Jinnai, T. Koga, Y. Nishikawa, T. Hashimoto, and S.T. Hyde, *Phys. Rev. Lett.* **78**, 2248 (1997).
- [43] H. Jinnai, Y. Nishikawa, and T. Hashimoto, *Phys. Rev. E* **59**, R2554 (1999).
- [44] H. Jinnai *et al.*, *Phys. Rev. Lett.* **84**, 518 (2000).
- [45] P.C. Hohenberg and B.I. Halperin, *Rev. Mod. Phys.* **49**, 435 (1977).
- [46] P. Debye, H.R. Anderson, and H. Brumberger, *J. Appl. Phys.* **28**, 679 (1957).
- [47] T. Otha, D. Jasnov, and K. Kawasaki, *Phys. Rev. Lett.* **49**, 1223 (1982).
- [48] M. Fiałkowski and R. Hołyst, *Acta Phys. Pol. B* **32**, 1579 (2001).
- [49] G. Brown and P.A. Rikvold, *Phys. Rev. E* **65**, 036137 (2002).
- [50] D. Anderson, H. Wennerström, and U. Olsson, *J. Phys. Chem.* **93**, 4243 (1989).
- [51] S.T. Hyde, B.W. Ninham, S. Anderson, Z. Blum, T. Landh, K. Larson, and S. Lidin, *The Language of Shape* (Elsevier, Amsterdam, 1997).
- [52] M. Takenaka and T. Hashimoto, *Physica A* **276**, 22 (2000).
- [53] <http://www.ichf.edu.pl/Dep3.html>